

Rydberg atom-enabled spectroscopy of polar molecules via Förster resonance energy transfer

Sabrina Patsch,¹ Martin Zeppenfeld,² and Christiane P. Koch¹

¹*Dahlem Center for Complex Quantum Systems and Fachbereich Physik, Freie Universität Berlin, Arnimallee 14, 14195 Berlin, Germany*

²*Max-Planck-Institut für Quantenoptik, Hans-Kopfermann-Straße 1, 85748 Garching, Germany*
(Dated: May 10, 2022)

Non-radiative energy transfer between a Rydberg atom and a polar molecule can be controlled by a DC electric field. Here we show how to exploit this control for state-resolved, non-destructive detection and spectroscopy of the molecules where the lineshape reflects the type of molecular transition. Using the example of ammonia, we identify the conditions for collision-mediated spectroscopy in terms of the required electric field strengths, relative velocities, and molecular densities. Rydberg atom-enabled spectroscopy is feasible with current experimental technology, providing a versatile detection method as basic building block for applications of polar molecules in quantum technologies and chemical reaction studies.

Cold polar molecules are an excellent platform for quantum control with applications ranging from fundamental physics [1, 2] and quantum information [3–5] to cold chemistry [6]. The ability to detect the molecules, ideally at the single molecule level and in a non-destructive and state-resolved fashion, is a prerequisite to any such application. Optical detection schemes such as laser-induced fluorescence or absorption [7–10] are destructive and difficult to apply at low density except for select molecules with optical cycling transitions. An alternative approach to non-destructive detection suggested use of Rydberg atoms [11, 12] – instead of driving molecular transitions by laser light, it exploits Förster resonant energy transfer (FRET), i.e., non-radiative energy exchange between donor and acceptor mediated by resonant dipole-dipole interaction [13, 14]. Rydberg atoms are particularly well suited to FRET due to their large dipole moment [15, 16]. Rydberg states are readily prepared [17, 18], and the scaling of Rydberg transitions with the principal quantum number [19] allows for covering the microwave and terahertz spectral range, i.e., rotational transition frequencies in a large variety of molecules [12]. Basic feasibility of non-destructive detection of molecules via FRET with Rydberg atoms has been demonstrated for ammonia [20], as has electric field control of the energy transfer [20–22]. The latter leverages the easy tunability of Rydberg energy levels, due to their sensitivity to external fields [23, 24]. The tunability suggests that FRET with a Rydberg atom may not only allow one to see whether a molecule is present or not but to actually infer the molecular state prior to the interaction. This would be an extremely useful tool for quantum technologies and studies of cold and ultracold chemistry but obviously requires a description of the molecular structure beyond the popular two-level approximation [4, 5, 12, 20–22, 25].

Here, we establish a theoretical framework from first principles for FRET in collisions of polar molecules and Rydberg atoms and predict electric field-dependent cross

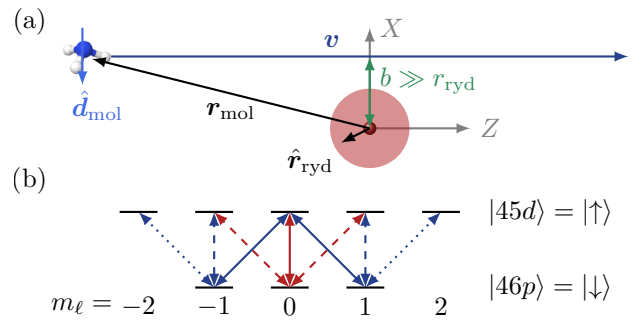


FIG. 1: (Colour online) Collision-mediated Rydberg spectroscopy of polar molecules relies on the interaction of the molecular dipole moment (lightblue arrow) with the electric field due to the charge distribution of the Rydberg atom’s valence electron (indicated by the shaded area). (a) Classical scattering trajectory (dark blue). (b) Relevant energy levels of the Rydberg atom with all possible dipole transitions indicated by arrows.

sections with full account of the interparticle dynamics. These cross sections will be obtained in an experiment by measuring the final state of the Rydberg atom via, e.g., ionization. The key parameter governing a collision is the relative velocity. We find that at sufficiently low relative velocity the cross sections display well-resolved lines as a function of electric field, with intricate lineshapes that encode the relevant selection rules. At very low velocity, linewidths below 1 MHz are achievable. Analysis of the peak heights and positions allows for inferring the state of the molecule or molecular ensemble. Such Rydberg spectroscopy of polar molecules only requires existence of (near) resonant dipole transitions in the two particles.

Theoretical framework — The different time and energy scales allow us to separate translational motion (which we treat classically) and internal degrees of freedom [26] similarly to the semi-classical impact parameter method [27]. The distance $\mathbf{r}_{\text{mol}}(t)$ between molecule

and atomic core, cf. Fig. 1(a), is then a time-dependent parameter in the atom-molecule interaction. The Hamiltonian for the internal degrees of freedom is given by

$$\hat{H}(t) = \hat{H}_{\text{ryd}} + \hat{V}_{\text{ryd}}^{\text{DC}} + \hat{H}_{\text{mol}} + \hat{V}_{\text{int}}(t), \quad (1)$$

where $\hat{V}_{\text{ryd}}^{\text{DC}}$ captures the Stark shifts in the Rydberg atom due to the DC electric field [35]. $\hat{V}_{\text{int}}(t)$ describes the interaction of the molecular electric dipole moment $\hat{\mathbf{d}}_{\text{mol}}$ with the electric field due to the charge distribution of the Rydberg atom's valence electron. For sufficiently large distances between atom and molecule, it is given by the dipole-dipole contribution,

$$\hat{V}_{\text{dd}}(t) = \frac{\hat{\mathbf{d}}_{\text{mol}} \cdot \hat{\mathbf{r}}_{\text{ryd}}}{r_{\text{mol}}^3(t)} - \frac{3(\hat{\mathbf{d}}_{\text{mol}} \cdot \mathbf{r}_{\text{mol}}(t))(\hat{\mathbf{r}}_{\text{ryd}} \cdot \mathbf{r}_{\text{mol}}(t))}{r_{\text{mol}}^5(t)}, \quad (2)$$

where $\hat{\mathbf{r}}_{\text{ryd}}$ is the position of the Rydberg electron. We assume the ensemble to be sufficiently dilute such that a Rydberg atom interacts at most once with a molecule [26] and neglect any change of the molecular trajectory due to the interaction,

$$\mathbf{r}_{\text{mol}}(t) = vt \mathbf{e}_Z + b \mathbf{e}_X \quad (3)$$

with $v \mathbf{e}_Z$ the velocity and b the impact parameter. Velocities down to about $v = 0.1$ m/s can be considered; for smaller velocities, the Rydberg atom is likely to decay before the particles had enough time to interact [26]. In Eq. (3), the molecular beam direction is parallel to the DC field but extension to other orientations of the trajectory is straightforward. The collision cross section for a given initial state $|\Psi_0\rangle$ of atom and molecule is obtained by integrating the probability $P_{\text{ex}}^{\Psi_0}(\Delta, b)$ for FRET to occur,

$$\sigma_{\Psi_0}(\Delta) = 2\pi \int_0^\infty b db P_{\text{ex}}^{\Psi_0}(\Delta, b). \quad (4)$$

Electric field tunability of the cross section arises from tuning the energy mismatch Δ via the Stark effect of the Rydberg atom.

Motivated by recent experiments [20, 22], we consider FRET between Rydberg atoms and the inversion mode of ammonia. The molecular state can be written in terms of the vibrational inversion mode $|\nu^\pm\rangle$ and the symmetric top eigenstates $|JKM\rangle$ [26]. Since rotational transition frequencies are large compared to the inversion splitting, it is sufficient to consider a single inversion doublet at a time, such that $|\nu^\pm JKM\rangle$ with $|\nu^+\rangle$ the lowest, symmetric and $|\nu^-\rangle$ the second lowest, anti-symmetric sub-level of the inversion doublet for given J , K and M . Coupling to other vibrational or electronic degrees of freedom is negligible. The inversion splitting depends on J and K approximately as [28]

$$\omega_{\text{inv}} = \omega_{\text{inv}}^0 - c_1 (J(J+1) - K^2 + c_2 K^2). \quad (5)$$

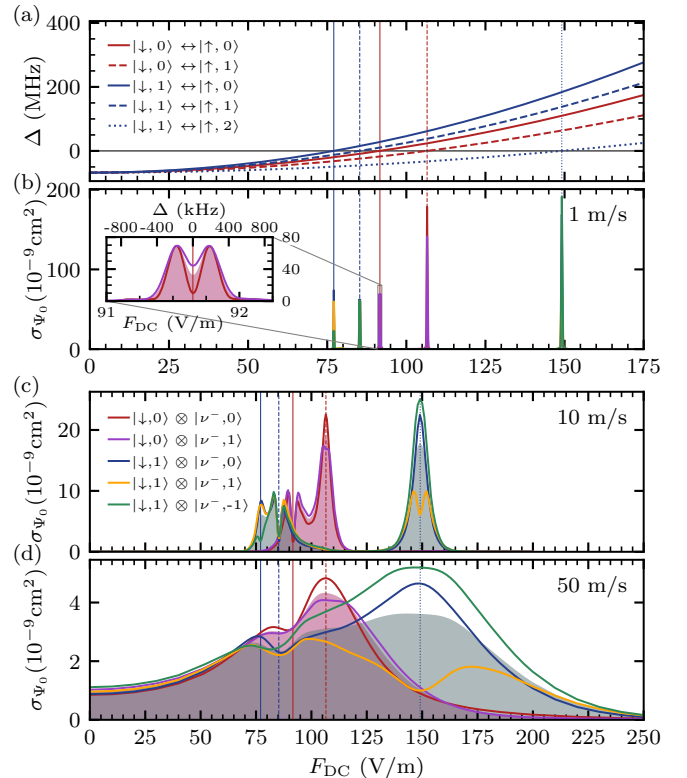


FIG. 2: (Colour online) Electric field control of collisions between molecules prepared in a single rotational energy level (here $J = 1 = K$) and Rydberg atom: (a) Energy mismatch Δ between the inversion mode of ammonia and the Rydberg transitions shown in Fig. 1(b). Vertical lines indicate resonances. (b-d) Cross sections for different initial states (indicated by line colour) and velocities (panels). Red (green) shaded areas show cross sections averaged over initial molecular states with the atom in $|\downarrow, 0\rangle$ ($|\downarrow, 1\rangle$). Note the different scales of the x- and y-axes.

with constants $c_{1,2}$ [28]. For fixed J and K , dipole transitions obey the selection rules $\nu^\pm \leftrightarrow \nu^\mp$ and $\Delta M = \pm 1$ or $\Delta M = 0$ (unless $M = 0 = M'$).

\hat{H}_{ryd} is represented in the spherical basis $|n\ell, m_\ell\rangle$ with principal quantum number n , angular quantum number ℓ and projection m_ℓ . Assuming rubidium, levels with $\ell \leq 7$ are shifted by the quantum defect $\delta_{n\ell j}$ due to the finite size of the ionic core [29]. We neglect spin-orbit coupling such that $\delta_{n\ell} \approx \delta_{n\ell, j=\ell+\frac{1}{2}}$. For low J and $K = J$, the inversion splitting of ammonia is matched by transitions between $|46p, m_\ell\rangle \equiv |\downarrow, m_\ell\rangle$ and $|45d, m'_\ell\rangle \equiv |\uparrow, m'_\ell\rangle$, cf. Fig. 1(b). For $J = K = 1$, the energy mismatch between the atomic and molecular transitions is shown in Fig. 2(a) as a function of the DC field strength. It vanishes at different field strengths for transitions involving different m_ℓ . This is at the core of the suggested spectroscopy.

Rydberg spectroscopy of polar molecules — We consider two different scenarios for spectroscopy. Both can be realized with existing experimental setups. In the first one, we assume the molecule to be prepared in a single rota-

tional energy level, for example in an experiment with a suitable (e.g. quadrupole) guide or Stark decelerator [30–32]. In the second scenario, we consider molecules in essentially arbitrary rotational states taking a thermal state as example and show that the cross sections allow for inferring that state. The two scenarios differ in the number of state-to-state cross sections that have to be averaged when predicting the outcome of an experiment. Both rely on FRET between atom and molecule and both assume state-resolved detection of the Rydberg atom after the collision.

Molecules in a single rotational level — We assume $J = K = 1$ for the molecule and the Rydberg atom in one of the states $|\downarrow, m_\ell\rangle$ with $m_\ell = 0, \pm 1$. Since the energy transfer is resonant, it is sufficient to consider only the upper inversion level for the molecule, $|\nu^-, M\rangle$ with $M = 0, \pm 1$. The cross section for all possible initial states is shown as a function of the DC field strength for three relative velocities in Fig. 2(b-d) with resonances indicated by vertical lines. As the velocity increases, the cross section peaks increase in width and decrease in amplitude. For dipole-dipole transitions, the maximum of the cross section and its line width scale as [12]

$$\max(\sigma) \sim d_{\text{mol}}/v, \quad \Delta \sim v^{3/2}/\sqrt{d_{\text{mol}}} \quad (6)$$

with $d_{\text{mol}} \sim K/\sqrt{J(J+1)}$ for the considered transition in symmetric top molecules [33]. In a molecular beam experiment, the molecules are randomly oriented, corresponding to an average over all M states. In contrast, atomic states with different m_ℓ are easily selected in the Rydberg state preparation. We thus consider two M -averaged cross sections, for $m_\ell = 0$ and $m_\ell = 1$ (shaded areas in Fig. 2(b-d)): At low velocities, the peaks do not overlap (Fig. 2(b)) and are clearly distinguishable also for higher velocities (Fig. 2(c)). While the resolution of single transitions is hampered at increasing velocity, the two M -averaged cross sections continue to be distinguishable up until about $v = 50$ m/s (Fig. 2(c)). In particular, the two resonances occurring at the largest field strengths, corresponding to $|\downarrow, m_\ell = 0; \nu^-, M\rangle \leftrightarrow |\uparrow, m_\ell = 1; \nu^+, M'\rangle$ for the dashed red and $|\downarrow, m_\ell = 1; \nu^-, M\rangle \leftrightarrow |\uparrow, m_\ell = 2; \nu^+, M'\rangle$ for the dotted blue vertical lines, can be resolved. It is thus possible to deduce the inversion splitting and hence the rotational level from the recorded cross-sections. At higher velocities, this is no longer the case.

The peak heights in Fig. 2(b-d) imply that an effective volume of $2 \cdot 10^{-9} \text{ cm}^3$ is probed by one Rydberg atom, assuming an interaction time of 100 μs . This suggests a fully saturated signal at a molecular density of $5 \cdot 10^8 \text{ cm}^{-3}$. In experiments, the molecular signal has to be discriminated against the background, mainly due to Rydberg transitions caused by blackbody radiation [20]. Given the cross sections in Fig. 2(b-d), this should be possible for densities as low as 10^5 cm^{-3} , cf. [26] for details.

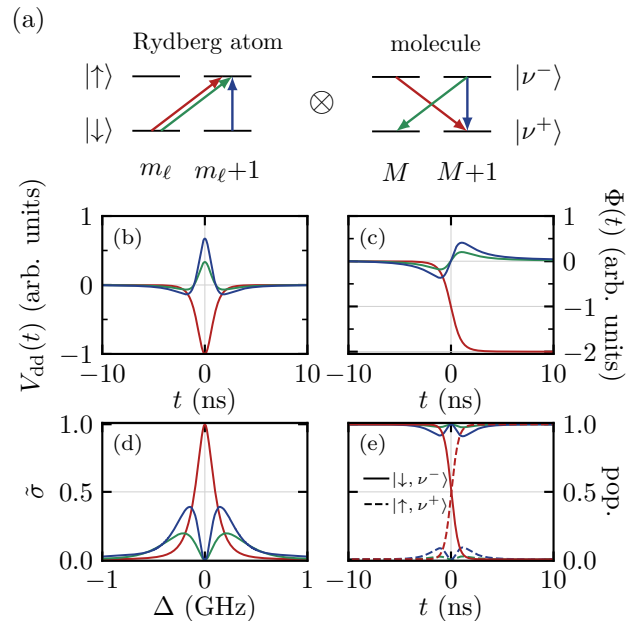


FIG. 3: (Colour online) Types of transitions in two two-level systems due to dipole-dipole coupling (a) and their behaviour during the collision (b-e). (b) interaction strength $\hat{V}_{\text{dd}}(t)$ scaled to a maximal absolute value of 1, (c) its integrated value $\Phi(t)$; (e) exemplary time evolution at resonance; (d) normalized cross-section $\tilde{\sigma} = \sigma/\sigma_{\text{max}}$ as a function of the energy mismatch Δ (with $\sigma_{\text{max}} = 1.7 \cdot 10^{-9} \text{ cm}^2$).

Various lineshapes are observed in Fig. 2(b-c), even in the M -averaged case. For example, if the Rydberg atom starts in $m_\ell = 0$ (vertical red lines), the cross section around 107 V/m (dashed) is Lorentzian but displays a clear dip around 92 V/m (solid, see inset). We now show that it is the time-dependence of the interaction (2) due to the collision that is reflected in the lineshape.

Understanding the lineshapes — The selection rules allow for three types of FRET transitions, cf. Fig. 3(a), which we term criss-cross (red), and linear (blue) and diagonal (green) flip-flop. In order to analyze each type separately, we reduce the Hilbert space of atom and molecule to only two states each, the ones connected by the respective transitions in Fig. 3(a). Then there is only a single matrix element for the interaction, $V_{\text{dd}}(t) = \langle \downarrow, m_\ell; \nu^-, M | \hat{V}_{\text{dd}}(t) | \uparrow, m'_\ell; \nu^+, M' \rangle$, shown in Fig. 3(b) for $v = 100$ m/s and $b = 160$ nm. It is symmetric as a function of time around $t = 0$ where the two particles are closest to each other and $V_{\text{dd}}(t)$ takes its extremal value. The two coupled two-level systems (TLS) accumulate a relative phase, which in the resonant case is simply given by $\Phi(t) = \int_{-\infty}^t V_{\text{dd}}(t') dt'$, shown in Fig. 3(c). For the criss-cross transitions (red lines), $V_{\text{dd}}(t)$ is always negative, $\Phi(t)$ thus decreases monotonically, the two TLS exchange their excitation perfectly (Fig. 3(e)), and the TLS cross section displays a Lorentzian peak (Fig. 3(d)). For

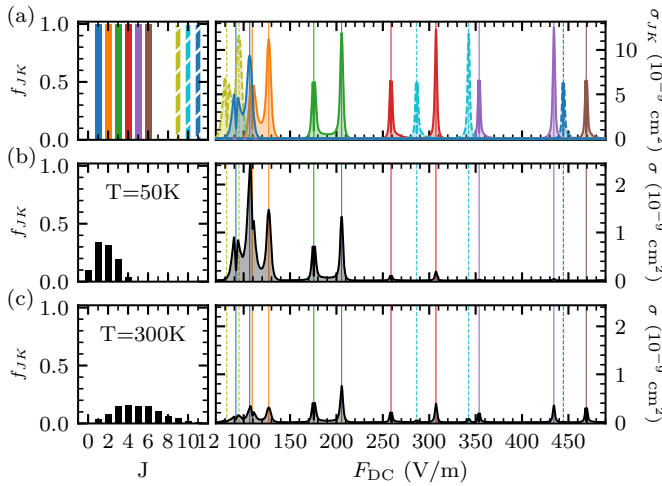


FIG. 4: (Colour online) Rubidium Rydberg spectroscopy of ammonia with M -averaged cross sections shown on the right (for $v = 10$ m/s and $m_\ell = 0$) and relative populations of the rotational states shown on the left for single rotational levels (a) and thermal ensembles (b,c) at rotational temperatures of 50 and 300 K, respectively. The vertical lines indicate resonances between the Rydberg transition and the inversion mode. Solid lines indicate $K = J$, dashed lines $K = J - 1$ (other molecular transitions are far off-resonant).

flip-flop transitions (green and blue lines in Fig. 3(b-e)), the non-Lorentzian lineshapes are rationalized by the different time evolution of $V_{dd}(t)$ with two changes of sign. Phase accumulation is then non-monotonic and, most importantly, the phase equals zero at $t = 0$. This causes the TLS to return to their initial states, cf. Fig. 3(e), resulting in a vanishing cross section at resonance. Shifting the transitions away from resonance breaks the symmetry in the time evolution of $V_{dd}(t)$, resulting in non-vanishing accumulated phase and cross section. This behavior is observed for both linear and diagonal flip-flop transitions since only the overall strength of their coupling differs.

While the cross sections in Fig. 2 arise from more complex dynamics than that of two coupled TLS, the peaks resemble lineshapes as seen in Fig. 3(d). For example, the peak at 107 V/m for the initial state $|\downarrow, m_\ell = 0\rangle \otimes |\nu^-, M = 1\rangle$ (purple line) is Lorentzian, suggesting a criss-cross transition where both m_ℓ and M change by one. Indeed, we numerically find the transitions to $|\uparrow, m_\ell = -1\rangle \otimes |\nu^+, M = 0\rangle$ to be dominant. In contrast, around 92 V/m, the peak shows a deep dip due to a flip-flop transition to $|\uparrow, m_\ell = 0\rangle \otimes |\nu^+, M = 1\rangle$. Note that the cross-section does not vanish entirely at resonance because our model includes all m_ℓ/M -sub-levels. Repeating this analysis for all initial states in Fig. 2 [26], we find all resonances to be dominated by one type of transition. The electric field controlled cross sections thus reveal whether a criss-cross or a flip-flop transition is at the core of a resonance.

Molecules in an ensemble of rotational states — We now discuss how to employ Rydberg spectroscopy to infer the population of molecular states. Figure 4 illustrates the working principle, correlating rotational states with peaks in the cross section. The dependence of the M -averaged cross section on the rotational quantum numbers J and K , shown in Fig. 4(a), can be observed as a function of the DC field strength, due to dependence of the inversion splitting on J and K , cf. Eq. (5). Figure 4 focusses on states with the Rydberg atom initially in $m_\ell = 0$ (for $m_\ell = 1$ see [26]) and molecules in $J \leq 11$ which have an inversion splitting near-resonant to the Rydberg transition at the considered electric field strengths and temperatures. The cross sections in Fig. 4(a) display a sequence of resonances, similarly to Fig. 2(b), with the position and height of the peaks depending on K , in perfect agreement with the scaling of Eq. (6). When considering a thermal ensemble, the cross sections are obtained by averaging over all states in the ensemble, cf. Fig. 4(b,c). The occupation of the rotational states is then given by $f_{JK}(T) = g/\mathcal{N}e^{-\frac{E_{JK}}{k_B T}}$ with T the temperature, \mathcal{N} a normalisation factor, and g the statistical weight of the state [26]. At very low temperatures, $T \leq 10$ K, the $J = K = 1$ contribution dominates, leading to a similar pattern as shown in Fig. 2(b). At higher rotational temperatures (Fig. 4(b,c)), an increasing number of rotational states contributes. For a relative velocity of $v = 10$ m/s, as shown in Fig. 4, the resonances are easily resolved and assigned to the different rotational states. The resonances for $J = 1, 2$ between 70 and 140 V/m are the hardest to resolve but Fig. 2 shows that this is possible until at least 50 m/s. Provided the velocity is sufficiently low for the peaks to be resolved, measurement of the cross section as a function of the electric field strength allows for inferring the rotational state composition of the molecular ensemble from the position and height of the peaks, for an example see [26]. In order to determine the composition of states with other K values, simply a different Rydberg transition has to be selected, e.g. $|47p, m_\ell\rangle$ to $|46d, m'_\ell\rangle$.

Conclusions — We have derived the principles of collision-mediated, non-destructive spectroscopy of polar molecules based on resonant dipole-dipole interaction with Rydberg atoms, using a complete dynamical description of the collision. Taking ammonia and rubidium as example, we have shown that electric field control of the cross sections allows for inferring the relative population of rotational states for velocities below 100 m/s. The lineshape reveals the dominant type of FRET-induced transition. For very low velocities, of the order of 1 m/s, linewidths below 1 MHz will be obtained. A key advantage of Rydberg atom-enabled spectroscopy is the ability to measure spectra for extremely low molecular density. Detection seem of single molecules in optical tweezers or

at molecular densities as low as 10^5 cm^{-3} seems realistic. Our example of ammonia and rubidium is easily carried over to other atomic and molecular species. Exchanging rubidium by helium [22], for instance, mainly reduces the quantum defects, rendering the isolation of a suitable dipole-dipole transition from neighbouring (possibly higher-order) transitions somewhat more difficult. When replacing ammonia by other polar molecules, purely rotational transitions can be used instead of the inversion mode [12]. A method for state-resolved non-destructive detection of polar molecules addresses an essential need for their application in quantum technologies and cold reaction dynamics studies and establishes Rydberg atoms as a versatile addition to the quantum control toolbox for cold and ultracold molecules [4, 5, 25].

We thank Ed Narevicius, Ronnie Kosloff, and Melanie Schnell for insightful discussions. Financial support from the Studienstiftung des deutschen Volkes e.V. and the Deutsche Forschungsgemeinschaft via the Priority Programme GiRyd (KO 2301/14-1 Grant No. 428456483) and Grant No. ZE 1096/2-1 is gratefully acknowledged.

-
- [1] N. R. Hutzler, *Quantum Science and Technology* **5**, 044011 (2020).
- [2] D. Mitra, K. H. Leung, and T. Zelevinsky, *Phys. Rev. A* **105**, 040101 (2022).
- [3] V. V. Albert, J. P. Covey, and J. Preskill, *Physical Review X* **10**, 031050 (2020).
- [4] K. Wang, C. P. Williams, L. R. B. Picard, N. Y. Yao, and K.-K. Ni, arXiv:2204.05293 (2022), URL <https://arxiv.org/abs/2204.05293>.
- [5] C. Zhang and M. R. Tarbutt, arXiv:2204.04276 (2022), URL <https://arxiv.org/abs/2204.04276>.
- [6] O. Dulieu and A. Osterwalder, eds., *Cold Chemistry*, Theoretical and Computational Chemistry Series (The Royal Society of Chemistry, 2018), ISBN 978-1-78262-597-1.
- [7] E. S. Shuman, J. F. Barry, D. R. Glenn, and D. DeMille, *Physical Review Letters* **103**, 223001 (2009).
- [8] D. Wang, B. Neyenhuis, M. H. de Miranda, K. K. Ni, S. Ospelkaus, D. S. Jin, and J. Ye, *Physical Review A* **81**, 061404(R) (2010).
- [9] L. W. Cheuk, L. Anderegg, B. L. Augenbraun, Y. Bao, S. Burchesky, W. Ketterle, and J. M. Doyle, *Phys. Rev. Lett.* **121**, 083201 (2018).
- [10] J. C. Shaw, J. C. Schnaubelt, and D. J. McCarron, *Phys. Rev. Research* **3**, L042041 (2021).
- [11] E. Kuznetsova, S. T. Rittenhouse, H. R. Sadeghpour, and S. F. Yelin, *Phys. Rev. A* **94**, 032325 (2016).
- [12] M. Zeppenfeld, *EPL (Europhysics Letters)* **118**, 13002 (2017).
- [13] T. Förster, *Annalen der Physik* **437**, 55 (1948).
- [14] D. L. Andrews and A. A. Demidov, *Resonance Energy Transfer* (Wiley, 1999).
- [15] K. A. Safinya, J. F. Delpech, F. Gounand, W. Sandner, and T. F. Gallagher, *Physical Review Letters* **47**, 405 (1981).
- [16] S. Ravets, H. Labuhn, D. Barredo, L. Béguin, T. Lahaye, and A. Browaeys, *Nature Physics* **10**, 914 (2014).
- [17] S. Haroche and J.-M. Raimond, *Exploring the Quantum. Atoms, Cavities, and Photons* (Oxford University Press, New York, 2006).
- [18] A. Larrouy, S. Patsch, R. Richaud, J.-M. Raimond, M. Brune, C. P. Koch, and S. Gleyzes, *Physical Review X* **10**, 021058 (2020).
- [19] N. Šibalić and C. S. Adams, in *Rydberg Physics* (IOP Publishing, 2018), pp. 1–27, ISBN 9780750316354.
- [20] F. Jarisch and M. Zeppenfeld, *New Journal of Physics* **20**, 113044 (2018).
- [21] V. Zhelyazkova and S. D. Hogan, *Phys. Rev. A* **95**, 042710 (2017).
- [22] K. Gawlas and S. D. Hogan, *Journal of Physical Chemistry Letters* **11**, 83 (2020).
- [23] A. Facon, E.-K. Dietsche, D. Grosso, S. Haroche, J.-M. Raimond, M. Brune, and S. Gleyzes, *Nature* **535**, 262 (2016).
- [24] C. S. Adams, J. D. Pritchard, and J. P. Shaffer, *Journal of Physics B* **53**, 012002 (2020).
- [25] E. Kuznetsova, S. T. Rittenhouse, I. I. Beterov, M. O. Scully, S. F. Yelin, and H. R. Sadeghpour, *Phys. Rev. A* **98**, 043609 (2018).
- [26] See supplemental material [url] for technical details, which includes Ref. [34].
- [27] I. Beigman and V. Lebedev, *Physics Reports* **250**, 95 (1995).
- [28] C. H. Townes and A. L. Schawlow, *Microwave Spectroscopy* (Dover Publications, Inc., New York, 1975).
- [29] T. F. Gallagher, *Rydberg atoms*, Cambridge Monographs on Atomic, Molecular, and Chemical Physics (Cambridge University Press, Cambridge, 1994).
- [30] L. Petitjean, F. Gounand, and P. R. Fournier, *Physical Review A* **33**, 143 (1986).
- [31] H. L. Bethlem, F. M. H. Crompvoets, R. T. Jongma, S. Y. T. van de Meerakker, and G. Meijer, *Physical Review A* **65**, 053416 (2002).
- [32] S. Chervenkov, X. Wu, J. Bayerl, A. Rohlfes, T. Gantner, M. Zeppenfeld, and G. Rempe, *Physical Review Letters* **112**, 013001 (2014).
- [33] H. W. Kroto, *Molecular Rotation Spectra* (John Wiley and Sons Ltd., New York, 1975).
- [34] N. Šibalić, J. D. Pritchard, C. S. Adams, and K. J. Weatherill, *Computer Physics Communications* **220**, 319 (2017).
- [35] The Stark effect of the molecule is negligible at the relevant field strengths [28].

Details on the molecular model

We consider FRET between Rydberg atoms and the inversion vibrational mode of ammonia. The latter can be modelled as a symmetric top rotor and its states can be described in terms of the symmetric top eigenstates $|JKM\rangle$. We use the standard notation with angular momentum quantum number J and projections onto the molecular symmetry axis K and onto the space-fixed Z -axis M [33]. The inversion mode then couples the $+K$ and $-K$ states. The rotational subspace with $J = K = 0$ does not possess an inversion mode and thus does not contribute to the FRET signal. At a given temperature, the occupation of the rotational states depends on J and K and is given by $f_{JK}(T) = g/\mathcal{N}e^{-\frac{E_{JK}}{k_B T}}$ with T the temperature, \mathcal{N} a normalization factor, and g the statistical weight of the state. The statistical weight is $g = 2(2J+1)$ except for $K = 3m$ with $m \geq 1$ where $g = 4(2J+1)$ due to the three-fold symmetry of ammonia [28].

Validity of the model

Our model relies on two basic assumptions — the translational motion can be treated classically, and the state of the Rydberg atom faithfully represents the Förster resonant energy transfer with the polar molecule. In the following, we assess the validity of these assumptions.

(1) The approximation of a classical, straight trajectory only remains valid as long as the kinetic energy E_{kin} is much larger than the interaction strength V_{dd} between the particles. The latter depends on the distance between the two particles. A suitable value for this distance in this context is impact parameter at which the population exchange between the particles is maximal, which we term the critical impact parameter. Its scaling with the relative velocity can be derived as follows. For the particles to exchange population, the phase accumulated by the particles, $\Phi = V_{\text{dd}}T$, needs to be of the order of one, $\Phi \sim 1$. The interaction scales as $V_{\text{dd}} \sim r^{-3}$ (cf. Eq. (2)) and the time during which the two particles interact significantly can be approximated as $T \sim r/v$. Combining the equations and solving for the critical impact parameter $r = b^*$ results in the scaling

$$b^* = \frac{c}{\sqrt{v}}. \quad (7)$$

The proportionality constant c is obtained from the numerical simulations by multiplying the impact parameter at which the exchange probability is maximal with the square-root of the velocity. We find the constant to be $c = 1.66 \cdot 10^{-6} \text{ m} \sqrt{\frac{\text{m}}{\text{s}}}$. For 0.1 m/s, the critical impact parameter amounts to $b^* = 5 \mu\text{m}$. We find that the condition for the energy scale separation is fulfilled with the kinetic energy, $E_{\text{kin}} = 180 \text{ kHz}$, being three orders of mag-

nitude larger than the interaction energy, $V_{\text{dd}} = 1.6 \text{ kHz}$. Only at relative velocities below $8 \cdot 10^{-6} \text{ m/s}$ will the two energies become equal (0.001 Hz).

(2) Furthermore, assuming a classical trajectory also relies on the de Broglie wavelength ($\lambda_B = h/\mu v$ with reduced mass μ) being much smaller than the distance between the particles. For 0.1 m/s, the critical impact parameter, $b^* = 5 \mu\text{m}$, is one order of magnitude larger than the de Broglie wavelength, $\lambda_B = 0.3 \mu\text{m}$. Only at relative velocities below $3 \cdot 10^{-4} \text{ m/s}$ will the de Broglie wavelength become equal to the critical impact parameter (100 μm).

(3) The duration of the experiment is limited by the lifetime of the Rydberg atom. For the Rydberg states considered in this work and at room temperature, the lifetime is mainly limited by decay processes induced by blackbody radiation and is around 75 μs (calculated using the *ARC* library [34]). The interaction time which is necessary for the particles to exchange a significant amount of population is easiest approximated when assuming a quasi-stationary setup in which the beginning and end of the experiment is defined by the excitation of the atom to the Rydberg regime and its ionisation. Using the critical impact parameter as derived above, the interaction time can be approximated as $T = \frac{2b^*}{v}$. Inserting Eq. (7), solving for v and inserting as interaction time the lifetime of the Rydberg atom, we obtain the critical velocity of 0.1 m/s. As a result, the model is mainly limited by the lifetime of the Rydberg atom and remains valid approximately until relative velocities of 0.1 m/s.

Approximation of necessary molecular densities

In the following, we elaborate on the estimation of the molecular density which required to detect the molecules via their interaction with Rydberg atoms. First, the effective volume that a Rydberg atom probes during a given time T can be approximated as $V = T v \sigma$. When inserting the peak values of the cross section from Fig. 2(b-d), for instance $\sigma \sim 2 \cdot 10^{-7} \text{ cm}^2$ at $v = 1 \text{ m/s}$, and assuming an interaction time of $T = 100 \mu\text{s}$, we obtain the value of $V = 2 \cdot 10^{-9} \text{ cm}^3$ as given in the main paper. This value is independent of v as σ scales as $1/v$, cf. Eq. (6). Second, at a molecular density ρ , the Rydberg atom interacts on average with $N = \rho V$ molecules. At a molecular density of $5 \cdot 10^8 \text{ cm}^{-3}$, the Rydberg atom then interacts on average with exactly one molecule and the signal is saturated. At higher densities, our approximation of a dilute medium breaks down. At lower densities, the signal reduces accordingly. When trapping, for instance, a single molecule in an optical tweezer with an estimated volume of 10^{-8} cm^3 , this corresponds to a density of 10^8 cm^{-3} and 20% of the saturated signal is achievable.

In a real experiment, these values have to be compared to the measured background. In the experiment [20], the

background is dominated by blackbody radiation which causes the Rydberg atom to change its state even if no molecules are present. During an interaction time of 100 μs , 2% of the Rydberg atoms can be found in $45d$ due to this effect. Therefore, at a molecular density of 10^7 cm^{-3} , the FRET signal and the background are of the same order of magnitude. This value can be further reduced by a few orders of magnitude: at 10^5 cm^{-3} , the FRET signal is hundred times smaller than the background but observing a change of 1% in the background transfer rate seems realistic. Of course, going to a setup with shielding of room temperature blackbody radiation, i.e., a cryogenic setup, would reduce the lower bound on the density for which molecules can be detected even further.

Detailed analysis of the peak structure in the electric field controlled cross section of Fig. 2

Figure 2 shows an intricate pattern of dips and peaks in the cross section as a function of the electric field. As discussed in the main text, the line shape can be traced back to the dominant transition occurring in the system. The possible kind of transitions, as discussed with the help of Fig. 3 in the main text, are summarised in Tab. I. This, together with the location of the resonance allows one to determine the dominant transition occurring in the combined system of Rydberg atom and molecule. (1) The peak position of resonance as a function of electric field strength reveals which transition occurs in the Rydberg atom as shown in Fig. 2(a). This gives the value of Δm_ℓ . (2) The line shape reveals whether a criss-cross or flip-flop transition occurs as shown in Tab. I. (3) Combining both, the value of ΔM can be concluded. We conduct this procedure in the following for all lines shown in Fig. 2.

In the main text, we have discussed as an example the initial state $|\downarrow, m_\ell = 0\rangle \otimes |\nu^-, M = 1\rangle$ (purple line in Fig. 2(b-d)). The dominant transitions are furthermore illustrated in Fig. 5(a). We found the peak at 107 V/m (corresponding to the resonance $|\downarrow, m_\ell = 0; \nu^-, M\rangle \leftrightarrow |\uparrow, m_\ell = \pm 1; \nu^+, M'\rangle$) being due to a criss-cross transition to $|\uparrow, m_\ell = -1\rangle \otimes |\nu^+, M = 0\rangle$ (purple dashed arrows in Fig. 5). The dip around 92 V/m ($|\downarrow, m_\ell = 0; \nu^-, M\rangle \leftrightarrow |\uparrow, m_\ell = 0; \nu^+, M'\rangle$), on the other hand, can be attributed to a linear flip-flop transition to $|\uparrow, m_\ell = 0\rangle \otimes |\nu^+, M = 1\rangle$

name	selection rule	line shape
criss-cross	$\Delta m_\ell = \Delta M = \pm 1$	peak
linear flip-flop	$\Delta m_\ell = \Delta M = 0$	dip
diagonal flip-flop	$\Delta m_\ell = -\Delta M = \pm 1$	dip

TABLE I: Overview of the types of transitions caused by dipole-dipole interaction.

(purple solid arrows in Fig. 5).

The initial state $|\downarrow, m_\ell = 0\rangle \otimes |\nu^-, M = 0\rangle$ (red) shows a qualitatively similar behaviour as $|\downarrow, m_\ell = 0\rangle \otimes |\nu^-, M = 1\rangle$ (purple), since the Rydberg atom is initially in the same state. At 107 V/m, criss-cross transitions with both $\Delta m_\ell = \Delta M = \pm 1$ are allowed (as indicated next to the red dashed arrows in Fig. 5(a)). Moreover, the linear flip-flop transition to $|\uparrow, m_\ell = 0\rangle \otimes |\nu^+, M = 0\rangle$, suggested by the dip at 92 V/m ($|\downarrow, m_\ell = 0; \nu^-, M\rangle \leftrightarrow |\uparrow, m_\ell = 0; \nu^+, M'\rangle$), is forbidden by the molecular selection rule $M = 0 \not\leftrightarrow M' = 0$ (as indicated by the red solid arrows in Fig. 5(a)). Instead, the molecule performs transitions with $\Delta M = \pm 1$ leading to a dip in the electric field controlled cross section.

The other three initial states correspond to the Rydberg atom being initially in $m_\ell = 1$ and thus relate to the resonances indicated by vertical blue lines in Fig. 2. The dominant transitions are illustrated in Fig. 5(b). We continue with the initial state $|\downarrow, m_\ell = 1\rangle \otimes |\nu^-, M = 0\rangle$ (blue). The cross section of this initial state shows a strong peak at the $|\downarrow, m_\ell = \pm 1; \nu^-, M\rangle \leftrightarrow |\uparrow, m_\ell = \pm 2; \nu^+, M'\rangle$ transition at 149 V/m. The line shape clearly indicates a criss-cross transition (i.e. $\Delta m_\ell = \Delta M = \pm 1$). The sign of the criss-cross transition can be deduced from the resonance itself which reveals that the Rydberg atom performs a transition from $46p, m_\ell = 1$ to $45d, m_\ell = 2$. Combining the two insights, we can deduce that the dominant transition occurs to the state $|\uparrow, m_\ell = 2\rangle \otimes |\nu^+, M = 1\rangle$ (dotted blue lines in Fig. 5(b)). The cross section also forms a peak around the resonance at 77 V/m ($|\downarrow, m_\ell = \pm 1; \nu^-, M\rangle \leftrightarrow |\uparrow, m_\ell = 0; \nu^+, M'\rangle$). Using similar arguments, the dominant transition is also a criss-cross transition to the state $|\uparrow, m_\ell = 0\rangle \otimes |\nu^+, M = -1\rangle$ (solid blue lines in Fig. 5(b)). Around the resonance at 85 V/m ($|\downarrow, m_\ell = \pm 1; \nu^-, M\rangle \leftrightarrow |\uparrow, m_\ell = \pm 1; \nu^+, M'\rangle$), the cross section forms a dip indicating a flip-flop transition. As the resonance indicates the Rydberg atom to perform a transition from $46p, m_\ell = 1$ to $45d, m_\ell = 1$, we can identify the linear flip-flop transition to $|\uparrow, m_\ell = 1\rangle \otimes |\nu^+, M = 0\rangle$ to be dominant (dashed blue lines in Fig. 5(b)). However, this transition is again forbidden by the molecular selection rule $M = 0 \not\leftrightarrow M' = 0$. Instead, the molecule performs transitions with $\Delta M = \pm 1$ which equally leads to a dip in the electric field controlled cross section.

The initial state $|\downarrow, m_\ell = 1\rangle \otimes |\nu^-, M = -1\rangle$ (green) shows a qualitatively very similar behaviour to $|\downarrow, m_\ell = 1\rangle \otimes |\nu^-, M = 0\rangle$ (blue), since similar transitions are involved. The only qualitative difference between the two occurs at the resonance around 77 V/m ($|\downarrow, m_\ell = \pm 1; \nu^-, M\rangle \leftrightarrow |\uparrow, m_\ell = 0; \nu^+, M'\rangle$). The green line forms dip here while the blue one forms a peak. The green state therefore performs a diagonal flip-flop transition to $|\uparrow, m_\ell = 0\rangle \otimes |\nu^+, M = 0\rangle$ (solid green lines in Fig. 5(b)).

Finally, the state $|\downarrow, m_\ell = 1\rangle \otimes |\nu^-, M = 1\rangle$ (yel-

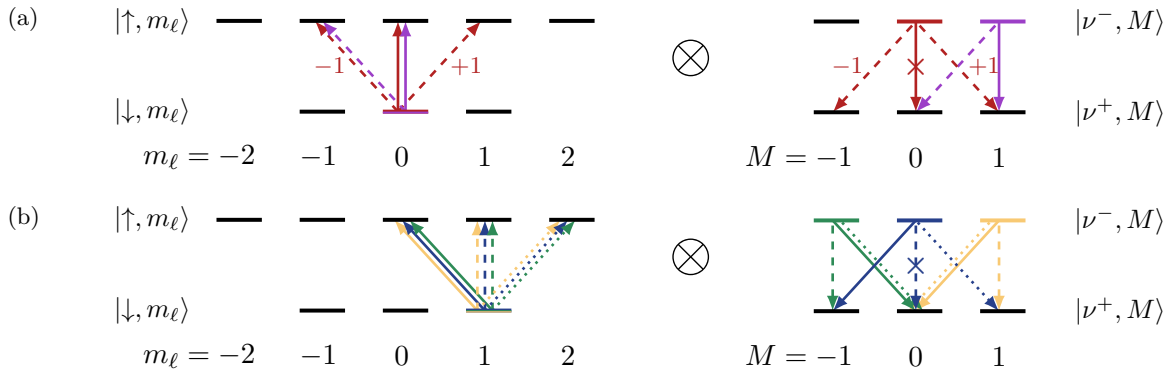


FIG. 5: Dominant transition in the combined system of Rydberg atom (left) and molecule (right) as shown in Fig. 2. (a) shows transitions for initial states with $m_\ell = 0$. Solid lines indicate the resonance $|\downarrow, m_\ell = 0; \nu^-, M\rangle \leftrightarrow |\uparrow, m_\ell = 0; \nu^+, M'\rangle$ which occurs at 92 V/m, dashed lines indicate the resonance $|\downarrow, m_\ell = 0; \nu^-, M\rangle \leftrightarrow |\uparrow, m_\ell = \pm 1; \nu^+, M'\rangle$ which occurs at 107 V/m. (b) shows transitions for initial states with $m_\ell = 1$. Solid lines indicate the resonance $|\downarrow, m_\ell = 1; \nu^-, M\rangle \leftrightarrow |\uparrow, m_\ell = 0; \nu^+, M'\rangle$ which occurs at 77 V/m, dashed lines indicate the resonance $|\downarrow, m_\ell = 1; \nu^-, M\rangle \leftrightarrow |\uparrow, m_\ell = 1; \nu^+, M'\rangle$ which occurs at 85 V/m, dotted lines indicate the resonance $|\downarrow, m_\ell = 1; \nu^-, M\rangle \leftrightarrow |\uparrow, m_\ell = 2; \nu^+, M'\rangle$ which occurs at 149 V/m. The line colours of the arrows indicate the initial state using the same colour code as in Fig. 2(b-d).

low) also shows a similar behaviour to $|\downarrow, m_\ell = 1\rangle \otimes |\nu^-, M = 0\rangle$ (blue), but deviates around the resonance at 149 V/m ($|\downarrow, m_\ell = \pm 1; \nu^-, M\rangle \leftrightarrow |\uparrow, m_\ell = \pm 2; \nu^+, M'\rangle$) as it shows a dip instead of a peak. Instead of a criss-cross, this state performs a diagonal flip-flop transition with $\Delta m_\ell = -\Delta M = 1$, driving the population to $|\uparrow, m_\ell = 2\rangle \otimes |\nu^+, M = 0\rangle$ (dotted yellow lines in Fig. 5(b)) and causing the strong dip in the spectrum.

It shall lastly be noted that cross sections do not completely vanish at resonance for flip-flop transitions (which form a dip) in the realistic model shown in Fig. 2, while in the simplified model of Fig. 3 they do. The reason is that for multi-level systems, the dynamics cannot be limited to a single transition. For instance, we have discussed that the initial state $|\downarrow, m_\ell = 1\rangle \otimes |\nu^-, M = 1\rangle$ (yellow state in Fig. 2) leads to a dip in the cross section at the $|\downarrow, m_\ell = \pm 1; \nu^-, M\rangle \leftrightarrow |\uparrow, m_\ell = \pm 2; \nu^+, M'\rangle$ transition at 149 V/m thus transferring population into $|\uparrow, m_\ell = 2\rangle \otimes |\nu^+, M = 0\rangle$. This state could further be transferred to $|\downarrow, m_\ell = 1\rangle \otimes |\nu^-, M = -1\rangle$ via a criss-cross transition. Thus, a fraction of the population is now in the state which we indicated by the green colour. In a second order process, this state can thus undergo a criss-cross transition leading to a peak at the considered $|\downarrow, m_\ell = \pm 1; \nu^-, M\rangle \leftrightarrow |\uparrow, m_\ell = \pm 2; \nu^+, M'\rangle$ transition which overlays with the initial dip created by the dominant flip-flop transition.

Molecules in an ensemble of rotational states for $m_\ell = 1$

We now present the dependence of the electric field controlled cross section on the rotational quantum num-

bers J and K assuming the Rydberg atom to be initially in $46P, m_\ell = 1$. This is equivalent to the results presented in the section “Molecules in an ensemble of rotational states” of the main paper but changing m_ℓ from 0 to 1. The results are shown in Fig. 6 where three resonances appear for each rotational state $|J, K\rangle$, giving rise to a richer spectrum as compared to $m_\ell = 0$. It can be seen that, different from Fig. 4, several peaks overlap, such as the green ($J = K = 3$) and the purple ($J = K = 5$) one around 290 V/m. However, this does not hamper the fitting procedure. Each rotational sublevel gives rise to at least one peak which is sufficiently isolated from the others in order to determine its contribution to the cross section. For instance, even the $J = K = 1$ state (blue) can be clearly identified at 50 K by its characteristic double-peak structure close to 85 V/m in Fig. 6(b).

Fitting the relative populations from measured cross sections

Measuring the electric field controlled cross section in an experiment allows for inferring the relative populations of rotational states. In the following, we sketch an example. First, we generate a noisy Boltzmann distribution which simulates an unknown distribution of rotational states in an experiment. We start from a Boltzmann distribution at 300 K (gray shade in left-hand panel of Fig. 7(b)) and add noise (red shade) by multiplying each component with a random number between 0 and 2, where a factor between 0 and 1 entails reduction and a factor between 1 and 2 increase of the corresponding component. We then re-normalise the distribution. When averaging the cross sections of single rotational

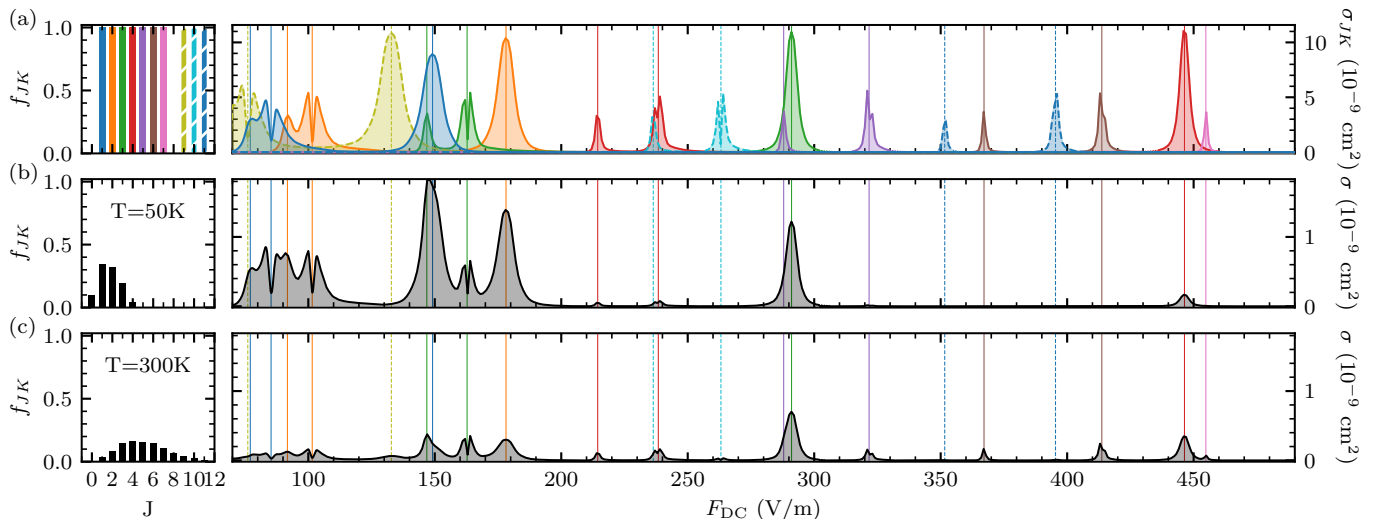


FIG. 6: Like Fig. 4 but for $m_\ell = 1$: Rubidium Rydberg spectroscopy of ammonia with M -averaged cross sections shown on the right (for $v = 10$ m/s and $m_\ell = 1$) and relative populations of the rotational states shown on the left for single rotational levels (a) and thermal ensembles (b,c) at rotational temperatures of 50 and 300 K, respectively. The vertical lines indicate resonances between the Rydberg transition and the inversion mode. Solid lines indicate $K = J$, dashed lines $K = J - 1$ (other molecular transitions are far off-resonant).

levels (cf. Fig. 7(a)) accordingly, we obtain the signal shown in Fig. 7(b, red line). This curve will serve as the unknown signal acquired in an experiment and will be the starting point for the fitting procedure. Note that we did not add any further disturbance to the signal to simulate experimental noise. In particular, we did not alter the peak positions or their shape but kept them as given in Fig. 7(a). We expect the theoretical prediction to be very accurate, since the theoretical model of the Rydberg atom and the rotation and inversion mode of the molecule are very well known.

We test two different strategies for acquiring the composition of rotational states by fitting the theoretical data from Fig. 7(a) to our test signal from Fig. 7(b, red). First, we use the full information on the state-dependent cross sections $\sigma_{JK}(F_{DC})$ as shown in Fig. 7(a) which have a very high resolution. The averaged cross section $\sigma(F_{DC})$ can be written as

$$\sigma(F_{DC}) = \sum_{JK} c_{JK} \sigma_{JK}(F_{DC}) \quad (8)$$

with $\sum_{JK} c_{JK} = 1$. We will treat the c_{JK} as fitting parameters which directly reflect the relative population of rotational states. Due to the resonance conditions, only 9 fitting parameters are left: c_{11} to c_{66} and c_{98} to c_{1110} . We perform the fit using the *optimize* package of

scipy with guess parameters $c_{JK} = 1$. The guess signal is therefore identical to the sum on the peaks in Fig. 7(a). We find that the fit recovers the input parameters exactly and the fitted curve lies exactly on top of the red line in Fig. 7(b).

To test the applicability of the fitting procedure to real experimental data, we reduce the resolution of the signal. Namely, we only consider data points which are located directly at the resonances as indicated by the black crosses in Fig. 7(b), thus reducing the number of data points to 16. Note that the signal is very low at some resonances because the line forms a dip around them. We repeat the fitting procedure with this decreased resolution and find the correct input parameters with a relative error of 10^{-16} . Note that, when dealing with very small signals in a real experimental setting, it might be beneficial to measure the cross sections slightly next to the resonance. This increases the signal-to-noise ratio when detecting cross sections which form a dip at the resonance.

This example demonstrates that the relative populations of rotational states can be inferred with a very high resolution from a given input signal. Of course, the error of the fitting procedure will ultimately be given by the error bars of the experiment.

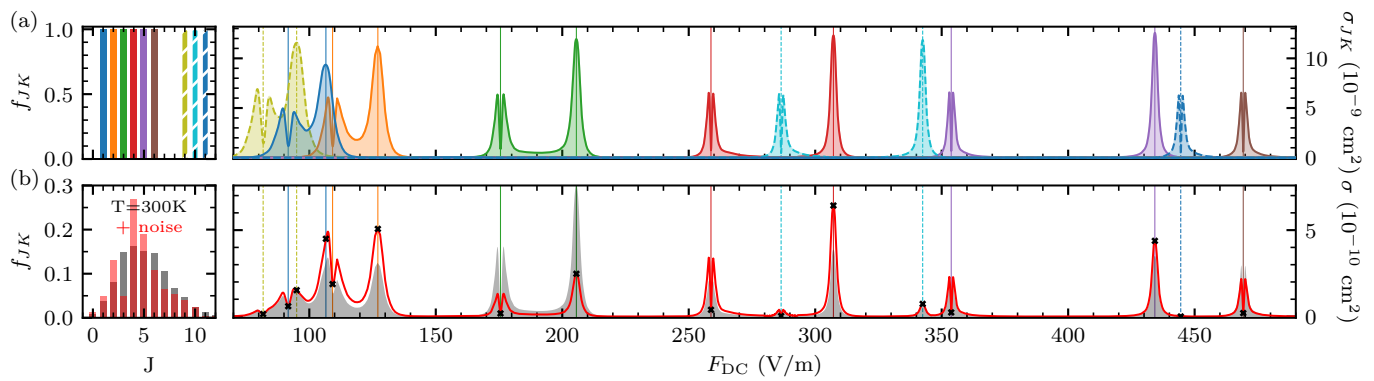


FIG. 7: Similar to Fig. 4: Rubidium Rydberg spectroscopy of ammonia for $v = 10 \text{ m/s}$ and $m_\ell = 0$. State-resolved cross sections are shown in (a), and (noisy) thermally averaged cross section in (b) panel. The red bar chart (b, left) and the red line (b, right) indicate the population distribution and corresponding cross sections when adding noise to a Boltzmann distribution with 300 K (black). The black crosses indicate the values used for fitting.